Antibunching dynamics of plasmonically mediated entanglement generation

Eugene Dumitrescu and Benjamin Lawrie
Quantum Computing Institute, Oak Ridge National Laboratory, Oak Ridge, Tennessee 37831, USA;
Quantum Information Science Group, Oak Ridge National Laboratory, Oak Ridge, Tennessee 37831, USA;
and Bredesen Center for Interdisciplinary Research, University of Tennessee, Knoxville, Tennessee 37996, USA
(Received 31 May 2017; published 10 November 2017; corrected 17 November 2017)

Dissipative entanglement-generation protocols embrace environmental interactions to generate long-lived entangled states. In this paper, we report on the antibunching dynamics for a pair of actively driven quantum emitters coupled to a shared dissipative plasmonic reservoir. We find that antibunching is a universal signature for entangled states generated by dissipative means and examine its use as an entanglement diagnostic. We discuss the experimental validation of plasmonically mediated entanglement generation by Hanbury Brown-Twiss interferometry with picosecond timing resolution determined by an effective two-qubit Rabi frequency, and we analyze the robustness of entanglement generation with respect to perturbations in local detunings, couplings, and driving fields.

DOI: 10.1103/PhysRevA.96.053826

I. INTRODUCTION

Quantum decoherence results from interactions with unknown or uncontrollable environmental degrees of freedom. This process, by which quantum information deteriorates due to environmental interactions, was coined information leakage [1]. It follows that quantum information processing systems should be completely isolated from leaky environments. However, such a task has proven to be quite difficult, and as a consequence, a variety of techniques were developed to combat the effects of decoherence [2]. With the fault tolerant threshold theorem [3] providing a route to overcome decoherence, quantum error correction protocols [2,4–9], dynamical decoupling protocols [10], and decoherence suppressing quantum control techniques [11,12] have all seen substantial progress.

Dissipative driven entanglement (DDE) techniques provide a different and complimentary route to quantum state engineering [13]. In this paradigm, entanglement is stabilized [14] and computations are performed [15] by leveraging select dissipative pathways that are naively assumed to impede long-term quantum coherence. Early experimental DDE progress has been achieved in trapped ion [16], atomic ensemble [17,18], and superconducting [19] qubit platforms.

Concurrently, a quantum information processing platform based on the quantum theory of plasmons has rapidly matured in recent years [20,21]. The first demonstration of plasmonically mediated entanglement [22] stimulated developments in both discrete [20] and continuous [23,24] plasmonic quantum variables. More recently, squeezed states of light have enabled ultratrace plasmonic sensing [25,26], while plasmonic mode volumes orders of magnitude below the diffraction limit have enabled Purcell factors exceeding 10^3 in the weak coupling limit [27] and vacuum Rabi splitting in the strong coupling limit [28,29]. These plasmonic analogs to photonic cavity QED provide a framework for the development of nanoscale architectures with ultrafast coupling dynamics capable of operation at ambient temperatures.

Despite substantial theoretical progress [30–42], dissipative entanglement generation has yet to be observed in plasmonic platforms. This is partially due to the technical difficulty of integrating plasmonic components with standard readout and control technologies. It is therefore tremendously important to develop alternative yet simple entanglement metrics to develop the nascent field of plasmonic quantum information processing. In this article we address this need by demonstrating how the second-order temporal correlation function can be used as a signature of entanglement between a pair of qubits coupled to a common plasmonic environment.

We analytically and numerically treat the dynamics of the dual quantum dot-plasmon hybrid system, illustrated in Fig. 1, and analyze the photon antibunching as a function of steady-state two qubit entanglement. We also argue that an experimental demonstration is possible, despite the fast qubit time scales inherited from the plasmonic reservoir. Importantly, we show that the two-qubit antibunching width can be classically tuned by controlling the external driving fields. Specifically, reducing local driving amplitudes slows the effective two-qubit Rabi frequency and extending the antibunching width to time scales as long as tens of picoseconds. Picosecond time scales are currently experimentally accessible and further, they are orders of magnitude shorter than typical coherence times observed in antibunching measurements of single quantum emitters (point defects, quantum dots, etc.). Antibunching lifetime measurements may therefore be used to distinguish between dissipative-driven entangled systems and weakly interacting single emitters.

II. THEORY

We consider a physical setup, illustrated in Fig. 1, consisting of a pair of qubits placed in close proximity to the near-field of a surface plasmon mode supported on a metallic nanowire. Qubit-qubit interactions are thus mediated by a plasmonic boson reservoir. The bare plasmon Hamiltonian is $H_{pls} = \int d\boldsymbol{r} \int_0^\infty d\omega \hbar\omega \hat{a}^\dagger(\boldsymbol{r},\omega)\hat{a}(\boldsymbol{r},\omega)$, where $\hat{a}(\boldsymbol{r},\omega)$ and $\hat{a}^{(\dagger)}(\boldsymbol{r},\omega)$ are the destruction and creation operators for elementary plasmonic excitations which satisfy bosonic commutation relations. A resonant or near-resonant mode may be treated as an oscillator $H_{pls} = \hbar\omega_a \hat{a}^\dagger\hat{a}$ with a principal frequency ω_a. The qubit Hamiltonian reads $H_i = \hbar\omega_i \hat{\sigma}_i^+\hat{\sigma}_i^-$, where $i = 0,1$ indexes the

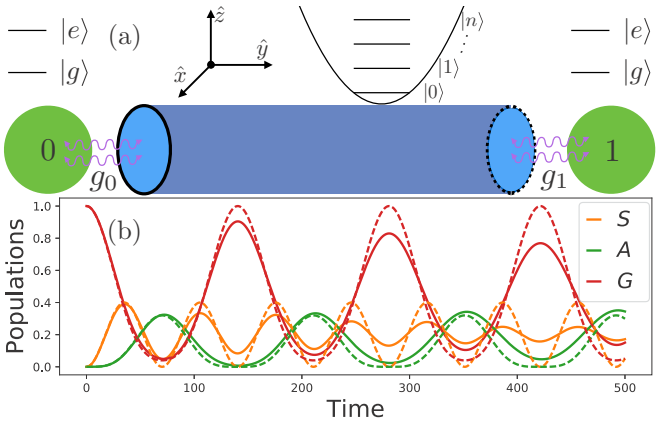

FIG. 1. (a) Schematic diagram of the setup described by Eq. (1). (b) Solid (dashed) lines show the numerical (effective analytic) populations of the ground (G), symmetric (S), and antisymmetric (A) states for a system with Hamiltonian parameters (and their effective counterparts without dissipation): $\Delta_0 = -\Delta_1 = 0.02$, $g_0 = g_1 = 0.02, \eta_0 = \eta_1 = 0.02$, and $\gamma_d = 2\gamma_r = 10^{-8}$. Hamiltonian parameters in all figures are expressed as ratios with respect to the dominant energy scale set by $\gamma_a = 50\,\mathrm{THz}$.

emitters which are modeled as two level systems (TLS) with $\hat{\sigma}_i^{\pm}$ being the Pauli ladder operators, $\hat{\sigma}^{\pm} = \hat{\sigma}^x \pm i\hat{\sigma}^y = |e\rangle\langle g|(|g\rangle\langle e|)$. The qubits could be implemented by a variety of solid-state platforms, for example, as semiconductor quantum dots [43,44]. We do not restrict ourselves to a specific qubit platform, but note that our results are generally applicable given appropriate plasmonic mode matching, which may be tuned by adjusting the nanowire geometry [45–47]. Defining the plasmonic and TLS dipole operators as $\hat{d}_a = \hat{a}^\dagger + \hat{a}$ and $\hat{d}_i = \hat{\sigma}_i^+ + \hat{\sigma}_i^-$, the emitter-reservoir coupling is modeled by the interaction $H_{\mathrm{int}} = \sum_i g_i \hat{d}_a \hat{d}_i$, where $g_i \equiv (\mu_i E_i)/\hbar$ is the dipole interaction strength in which we absorbed all physical constants, i.e., the emitter transition dipole moment μ_i and local plasmon electric field magnitude $E_i = \sqrt{\frac{\hbar\omega_a}{2\epsilon_0 V}}$, where V is the plasmon mode volume. Plasmonic elements behave as lossy electromagnetic cavities in the both the weak and strong QED regimes [21,27–30,47]. Finally, $H_D = -\sum_i(\eta_i e^{i\Omega_i t}\hat{\sigma}_i^+ + \mathrm{H.c.}) - (\eta_a e^{i\Omega_a t}\hat{a}^\dagger + \mathrm{H.c.})$ models transitions being driven by external fields with amplitudes $\eta_{i(a)}$ and frequencies $\Omega_{i(a)}$. Transforming to the corotating reference frame, with detunings $\Delta_{i(a)} = \hbar(\omega_{i(a)} - \Omega_{i(a)})$, and applying the rotating wave approximation, the total Hamiltonian becomes

$$H_{\mathrm{tot}} = \sum_{i=0,1}[\Delta_i \hat{\sigma}_i^+\hat{\sigma}_i^- - \eta_i\hat{d}_i - g_i(\hat{\sigma}_i^+\hat{a} + \hat{\sigma}_i^-\hat{a}^\dagger)] + \Delta_a\hat{a}^\dagger\hat{a} - \eta_a\hat{d}_a. \quad (1)$$

Dissipation is modeled by treating the dynamics within the Lindblad master equation formalism

$$\dot{\rho} = -i[H_{\mathrm{tot}},\rho] + \sum_k \gamma_k\left(L_k\rho L_k^\dagger - \frac{1}{2}\{L_k^\dagger L_k,\rho\}\right), \quad (2)$$

where we take $\hbar = 1$ and the L_k operators model various dissipative channels. Specifically, we consider the following channels: (i) plasmonic relaxation $L_a \equiv \hat{a}$ at a rate $\gamma_a \leqslant 50\,\mathrm{THz}$ [48], (ii) emitter relaxation $L_{r,i} \equiv \hat{\sigma}_i^+$ at a rate $\gamma_r = 2.5\,\mathrm{MHz}$, and (iii) emitter dephasing $L_{d,i} \equiv \hat{\sigma}_i^z$ at a rate $\gamma_d = 5\,\mathrm{MHz}$. Later we numerically solve Eq. (2) in full to validate antibunching and concurrence phenomenon in a wide range of parameter regimes. However, we first derive an effective model to develop our intuition of the dynamics.

III. TWO-QUBIT EFFECTIVE DYNAMICS

Let us now illustrate the dissipative flow dynamics for two qubits coupled through a common bosonic reservoir. Both the effective model and our exact numerical calculations will identify the antisymmetric singlet state $|A\rangle = |eg\rangle - |ge\rangle$ as a fixed point for the dynamical evolution in the parameter regimes highlighted below. For our effective model, we work in the weak coupling regime defined by $g_0, g_1, \eta_0, \eta_1 \ll \gamma_a$, where γ_a is the rate for the relaxation channel taken with the relaxation time scale $\tau_a = 1/(\pi * \gamma_a) \sim 6\,\mathrm{fs}$. In this work we stay within this approximation so all energy and time scales are given as dimensionless ratios of γ_a. Still, the reservoir dynamics enables coherent communication channel between the distant qubits. As we now show, the system may be guided into the decoherence free subspace $|A\rangle$ by varying the qubits detunings and drivings in Eq. (1), or equivalently, by driving the bosonic reservoir [42].

The effective qubit dynamics is found by the following adiabatic elimination procedure [42]. From Eqs. (1) and (2) the Heisenberg equations of motion for the field operators are

$$\begin{aligned}\dot{\sigma}_i^z &= i[2g_i(\sigma_i^+ a - \sigma_i^- a^\dagger) + 2\eta_i(\sigma_i^+ - \sigma_i^-)] \\ &\quad - \gamma_i(\mathbb{I} - \sigma_z) + f_i^z, \\ \dot{\sigma}_i^- &= -i\left[\Delta_i\sigma_i^- + (g_i a + \eta_i)\sigma_i^z\right] - \gamma_i\sigma_i^-/2 + f_i^-, \\ \dot{a} &= i[\eta_a - \Delta_a a + g_0\sigma_0^- + g_1\sigma_1^-] - \gamma_a a/2 + f_a,\end{aligned} \quad (3)$$

with fluctuation operators f_i^z, f_i^-, f_a representing higher-order processes [42]. Making the semiclassical approximation that expectation values for the fluctuation operators vanish, we decouple the expectation values of the qubits and the bosonic mode. For slowly varying $\langle a\rangle$, valid in the case of weak coupling and drivings, we may set $\dot{a} = 0$ and substitute the resulting expression into the the first two lines of Eq. (3). This gives us the adiabatic Heisenberg equations of motion, which can, in turn, be viewed as arising from an effective two-qubit Hamiltonian with nonlocal dissipation terms. The effective Hamiltonian, $H_{qb} = \sum_i[\tilde{\Delta}_i\hat{\sigma}_i^+\hat{\sigma}_i^- - \tilde{\eta}_i\hat{d}_i] - \tilde{g}(\hat{\sigma}_0^+\hat{\sigma}_1^- + \hat{\sigma}_1^+\hat{\sigma}_0^-)$ is defined in terms of the following couplings: (i) effective local detunings $\tilde{\Delta}_i = \Delta_i - g_i^2\Delta_a/Z$, (ii) effective driving fields $\tilde{\eta}_i = \eta_i + g_i\Delta_a\eta_a/Z$, and (iii) effective interqubit coupling $\tilde{g} = g_0 g_1\Delta_a/Z$, where $Z = (\gamma_a/2)^2 + \Delta_a^2$. The effective dissipations are described by $\sum_{ij=0,1}\tilde{\gamma}_{ij}/2[2\sigma_i^-\rho\sigma_j^+ - \{\sigma_j^+\sigma_i^-,\rho\}]$, with single-qubit relaxations occurring at a renormalized rate $\tilde{\gamma}_{ii} = \gamma_i + g_i^2\gamma_a/Z$ and collective reservoir mediated relaxations occurring at the rate $\tilde{\gamma}_{ij} = g_0 g_1\gamma_a/Z$. Transforming to the Dicke basis, $|E\rangle = |ee\rangle \equiv |s = 1, m = 1\rangle$, $|S\rangle = |eg\rangle + |ge\rangle$, $|A\rangle = |eg\rangle - |ge\rangle$, $|G\rangle = |gg\rangle$, and defining the effective (anti)symmetric drivings $\eta_\pm = (\tilde{\eta}_0 \pm \tilde{\eta}_1)/\sqrt{2}$ and energies $\Delta_\pm = (\tilde{\Delta}_0 \pm \tilde{\Delta}_1)/2$. Note that $|A\rangle$ is the part of the two-qubit space while

$|G\rangle,|S\rangle,|E\rangle$ define the triplet basis vectors defined by angular momentum eigenvalues $m = -1,0,1$, respectively.

The Hamiltonian now reads

$$\begin{aligned} H_D = {} & \Delta_E|E\rangle\langle E| + \Delta_S|S\rangle\langle S| + \Delta_A|A\rangle\langle A| \\ & + \Delta_-(|A\rangle\langle S| + |S\rangle\langle A|) \\ & - \eta_-(|S\rangle\langle G| + |S\rangle\langle E| + \text{H.c.}) \\ & - \eta_+(|A\rangle\langle G| - |A\rangle\langle E| + \text{H.c.}), \end{aligned} \tag{4}$$

where $\Delta_E = 2\Delta_+$, $\Delta_S = \Delta_+ + \tilde{g}$, and $\Delta_A = \Delta_+ - \tilde{g}$.

As a special case, we take antisymmetric detunings and identical drivings, thus reducing the effective parameters to $\tilde{\Delta}_i = \Delta_i$, $\tilde{\eta}_i = \eta_i$, $\tilde{g} = 0$, $\tilde{\gamma}_{ii} = \gamma_i + 4g_i^2/\gamma_a$, and $\tilde{\gamma}_{ij} = 4g_0g_1/\gamma_a$. The resulting pure-state populations, e.g., with $\rho(0) = |G\rangle\langle G|$, oscillate with an effective two-qubit Rabi frequency $\Omega = \sqrt{(\Delta/2)^2 + \eta^2}$ as $\rho_E(t) = [\Delta^2 + \eta^2\cos(2t\Omega) - \Omega^2]^2/4\Omega^4$, $\rho_S(t) = \eta^2\sin^2(2t\Omega)/2\Omega^2$, $\rho_A(t) = 2\Delta^2\eta^2\sin^4(t\Omega)/\Omega^4$, $\rho_G(t) = (\Delta^2 + \eta^2\cos(2t\Omega) + \Omega^2)^2/4\Omega^4$, and are illustrated by the dashed lines in Fig. 1.

The solid populations in Fig. 1 are calculated by numerically solving Eq. (2) for the full system and can be understood as follows. As discussed above, the excited state $|E\rangle$ relaxes to the singly excited state $|eg(ge)\rangle$ at a rate $\tilde{\gamma}_{00(11)}$. However, in the Dicke basis, relaxation from the bi-excited state to the symmetric (antisymmetric) state occurs at the rate $\gamma_{S(A)} = \sum_i \tilde{\gamma}_{ii}/2 \pm \gamma_{ij}$. Ignoring Hamiltonian dynamics for the moment, the populations are coupled as $\dot{\rho}_{SS} = (\rho_{EE} - \rho_{SS})\gamma_S$ and $\dot{\rho}_{AA} = (\rho_{EE} - \rho_{AA})\gamma_A$. Thus, the solid lines in Fig. 1 and the eventual steady states are driven by symmetric pumping described by Eq. (4) augmented by super and subradiant dissipation from the states $|S\rangle$ and $|A\rangle$, respectively. As discussed below, the entangled state $|A\rangle$ is a fixed-point solution to these dynamics.

We now explore steady-state characteristics as a function of the parameter space defined in Eq. (1). Fixed-point entanglement is characterized by Wooter's concurrence C [49]. The concurrence of a two-qubit state ρ is $C(\rho) = \max\{0,\lambda_1 - \lambda_2 - \lambda_3 - \lambda_4\}$ where λ_j are the sorted eigenvalues of $\rho\tilde{\rho}$, with the spin-flipped conjugate state $\tilde{\rho} = \sigma_1^y\sigma_2^y\rho^*\sigma_2^y\sigma_1^y$. C ranges between 0, for product states, and 1, for maximally entangled states. As indicated by our earlier discussion and illustrated in Fig. 2, unit concurrence is readily achievable for systems with approximately equal couplings and driving fields as well as approximately antisymmetric qubit detuning. In all cases, the pair of qubits evolves to the antisymmetric entangled state $|A\rangle$ [40,42].

IV. $g^{(2)}(\tau)$ AS AN ENTANGLEMENT WITNESS

We now investigate the use of the second-order temporal correlation function to quantify entanglement generation in our system. Entanglement is typically validated by an ensemble of computational basis state measurements that are classically postprocessed to either perform state tomography [51,52] or demonstrate a quantum inequality violation [53,54]. Tomographic state readout has been successfully performed for dissipatively entangled trapped ions [16] using specialized readout mechanisms. However, for nascent plasmonic technologies, it is worthwhile to develop simple experimental signatures consistent with entangled states, without the complicated readout electronics needed to perform full-state tomography.

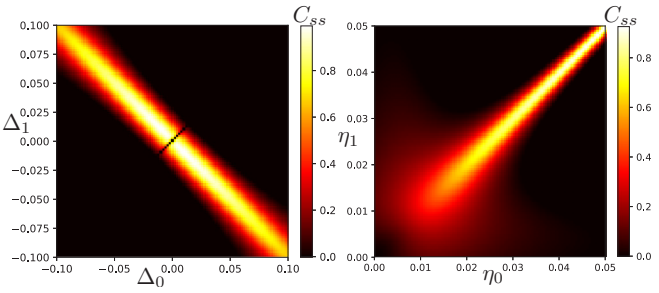

FIG. 2. Heat map of steady-state concurrence C_{ss} as a function of (left) qubit detunings $\Delta_{0,1}$ with equal qubit drivings $\eta_0 = \eta_1 = 0.05$ and (right) qubit driving amplitudes $\eta_{0,1}$ with asymmetric qubit detunings $\Delta_0 = -\Delta_1 = 0.01$. Symmetric drivings and couplings with antisymmetric detunings yields near unity concurrence steady states $\rho_{ss} \approx |A\rangle\langle A|$. Parameters common to both panels are coupling strengths $g_0 = g_1 = 0.05$ and plasmon detuning and driving $\Delta_a = \eta_a = 0$.

In this context, antibunching in $g^{(2)}(\tau)$ of emitted light was suggested as an alternative entanglement signature [40,55,56]. Below we confirm that the second-order correlation function successfully discriminates between entangled, arising in the form $|A\rangle$, and unentangled steady states generated by our protocol. Importantly, antibunching by itself is not conclusive evidence of entanglement between qubits with a shared dissipative pathway. For instance, if both qubits were not well coupled to the same plasmonic mode, steady-state entanglement would not be generated, but each qubit would exhibit antibunching on a time scale determined by the lifetime of the qubit. By considering the antibunching dynamics, it is possible to distinguish antibunching due to individual uncoupled emitters and antibunching due to dissipative, driven, entanglement between qubits coupled to a shared plasmonic reservoir.

The second-order correlation function measures the degree to which a system is temporally correlated. For stationary processes invariant under time translation, as is the case for steady states, the correlation function is defined as

$$g^{(2)}(\tau) = \frac{\langle a^\dagger(t)a^\dagger(t+\tau)a(t+\tau)a(t)\rangle}{\langle a^\dagger(t)a(t)\rangle^2}. \tag{5}$$

In the context of quantum optics, $g^{(2)}(\tau)$ has the simple and intuitive interpretation of the normalized probability that two photons, whose emission times differ by τ, are detected at a point in space. A Hanbury-Brown-Twiss (HBT) interferometer [57] can be used to measure this quantity. In a modern HBT interferometer, a 50/50 beamsplitter is used to send a light source to a pair of single-photon counting detectors, and high-speed electronics tag the arrival times of photons at each detector, with temporal resolution as fast as 1 picosecond.

To calculate $g^{(2)}(\tau)$, let us now combine continuous time evolution with a discrete quantum jump model. Consider a steady state ρ_{ss} of Eq. (2), whose concurrence is plotted in Fig. 2, which spontaneously emits a single photon from either qubit. An emission event originating from the ith qubit

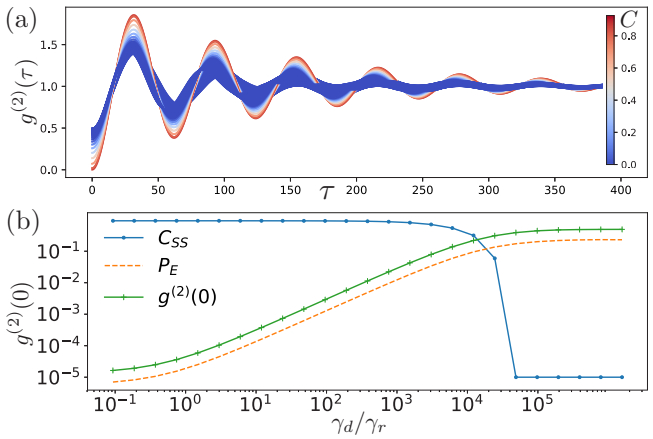

FIG. 3. The steady-state $g^{(2)}(\tau)$ correlation function as driving amplitudes $\eta_1 = 0.05$ and η_0 varies across [0.04,0.06]. The blue traces in panel (a) correspond to statistical mixtures of $|gg\rangle$ and $|eg(ge)\rangle$ depending on the circle endpoints. These states showing a $g^{(2)}(0) = 0.5$ and correspond to general mixed states. Over this range the concurrence evolves (see color bar labeled by C) from 0, where $g^{(2)}(0) = 1/2$, to 1, where $g^{(2)}(0) = 0$. Other Hamiltonian parameters, as ratios of γ_a, are $\Delta_0 = -\Delta_1 = 0.02$, $g_0 = g_1 = 0.05$, and $\eta_1 = 0.05$. τ is presented in units of $1/(\pi * \gamma_a) \approx 6$ fs.

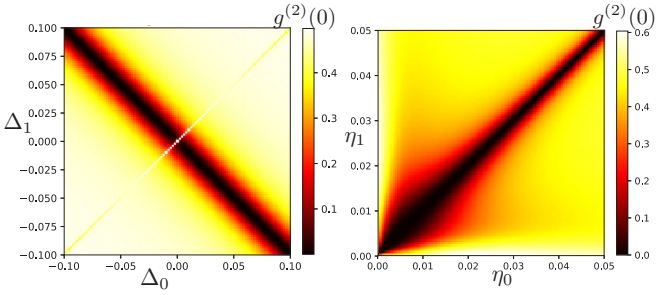

FIG. 4. Zero-delay correlations $g^{(2)}(0)$ as a function of (left) qubit detunings $\Delta_{0,1}$ and (right) qubit drive amplitudes $\eta_{0,1}$ using parameters reported in Fig. 2. Dark bands, which overlap strongly with the high concurrence regions, denote parameter regimes for which antibunching is present.

corresponds mathematically to the application of a destruction operator σ_i^- which projectively maps the postemission state to $\rho_i(0) = \hat{\sigma}_i^{(-)}\rho_{ss}\hat{\sigma}_i^{(+)}/\mathrm{Tr}[\hat{\sigma}_i^{(-)}\rho_{ss}\hat{\sigma}_i^{(+)}]$. Defining $\rho_i(\tau)$ as $\rho_i(0)$ evolved from $t = 0$ to $t = \tau$ according to Eq. (2), the probability for a second emission from the jth qubit at time τ is then $\mathrm{Tr}[\hat{n}_j\rho_i(\tau)]$, where $\hat{n}_j = \hat{\sigma}_j^{(+)}\hat{\sigma}_j^{(-)}$ is the qubit number operator. Tracing over all emission configurations gives us the correlation function

$$g^{(2)}(\tau) = \sum_{ij} \mathrm{Tr}[\hat{n}_j\rho_i(\tau)]. \tag{6}$$

Figure 3(a) illustrates the behavior of $g^{(2)}(\tau)$ when the driving amplitude η_0 varies across [0.04,0.06]. Across this range, the concurrence varies from 0 to 1, and back to 0, as denoted by the color of the curves (also see Fig. 2). At unity concurrence we observe that $g^{(2)}(0) = 0$, while for unentangled states, marked by vanishing concurrence, the zero-delay correlations saturate to $g^{(2)}(0) \sim 0.5$. Generally, this correlated antibunching signature appears for all dissipatively generated entangled steady states, as can be seen by comparing Figs. 2 and 4.

It is interesting and necessary to study the effects of generic decoherence with respect to entanglement generation and antibunching. For example, we consider dephasing noise which is modeled by the presence of dephasing channels acting locally on each qubit. In Fig. 3(b) we vary the strength of the dephasing noise with respect to the relaxation rate and plot the steady-state concurrence, zero-delay signal, and population of the dually excited state $|E\rangle = |ee\rangle$.

We emphasize that the observation of an antibunching dip is not a general entanglement metric for arbitrary quantum states. However, it is a universal feature shared by subradiance-generated entangled steady states in our setup. It is worth noting that antibunching is routinely observed in experiments involving single quantum emitters. The antibunching from single quantum emitters is rooted in the fact that after emitting a photon the emitter relaxes to its ground state and cannot source another photon without some time passing for the emitter to become excited again. For single quantum emitters, the antibunching dip width is proportional to the bare emitter decay rate (γ_r). Below we discuss how the width of the antibunching emanating from a pair of emitters, which are coupled by a common plasmonic reservoir, is many orders of magnitude smaller than a signal being sourced by a single quantum emitter.

Note that the robustness of the antibunching signal is rooted in the fact that, similar to the single emitter case, a single quantum is shared between two qubits in the form of the state $|A\rangle$. Antibunching could also be caused by product states sharing a single quantum, e.g., $|eg\rangle$ or $|ge\rangle$, but these are unstable under the dynamics considered and the time scales would be quite different as already mentioned. Further, $g^{(2)}(\tau)$ is unaffected by states including statistical mixtures of $|G\rangle$ (which do not contribute any emissions), while the bi-excited state $|E\rangle$ may generate two emission events with a small delay with high probability. These dual emissions destroy the antibunching signal. Antibunching is therefore maximal in our setup for the only stable single excitation subspace: $|A\rangle$.

While antibunching is an attractive entanglement signature due to its simplicity, its observation is nontrivial due to the fast time scales inherited from the plasmonic reservoir. After each radiative decay event, the two-qubit system flows back to its steady-state solution as described earlier. Hence the width of the $g^{(2)}(0)$ antibunching dip is inversely proportional to the population oscillation Rabi frequency Ω. Tunable driving frequencies are therefore critical to observing antibunching on experimentally accessible time scales. While nonlinear mixing with femtosecond laser sources could enable the detection of subpicosecond dynamics in $g^{(2)}(\tau)$, conventional HBT interferometry is limited by the 1-ps temporal resolution of state-of-the-art time tagging electronics. To that end, we numerically calculate the oscillation time scales by Fourier transforming the $g^{(2)}(\tau)$ signal into the frequency domain and identifying the characteristic driving frequency, which fixes the antibunching time scale. The time scales are provided in the Fig. 5 color maps, as a function of detuning and driving amplitudes, with normalized time in units of $T = 1/(\pi * \gamma_a) \approx 6$ fs reported in the color legend. Antibunching time scales in the $\sim$10 ps range for entangled states are

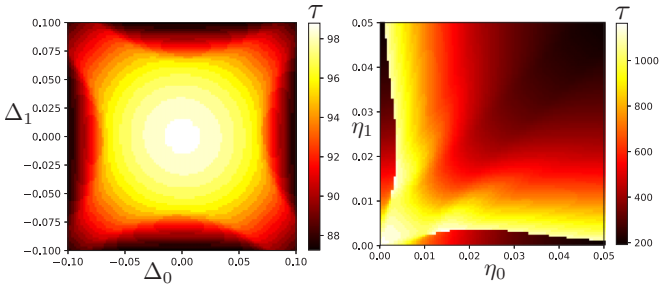

FIG. 5. Oscillation time scales for antibunching signal as a function of (left) qubit detunings $\Delta_{0,1}$ and (right) qubit drive amplitudes $\eta_{0,1}$. Time scales reported are in units of $T = 1/(\pi * \gamma_a) \approx 6$ fs with remaining parameters as in Fig. 2. Entangled region around $\eta_0 = \eta_1 = 0.03$ displays a characteristic bunching time scale $T_{AB} \sim 10$ ps.

easily experimentally realizable, e.g., for small driving fields around $\eta_0 = \eta_1 \approx 0.03$. Notably, these timescales are much shorter than the lifetimes of typical qubits. For instance, nitrogen-vacancy (NV) centers in diamond have lifetimes of order 10–30 ns [50].

V. CONCLUSION AND DISCUSSION

In this paper we examine the entanglement characteristics of steady states generated by a pair of qubits subject to a dissipative plasmonic reservoir. We find that maximally entangled steady states are routinely achievable by appropriately tuning qubit detunings, couplings, and driving frequencies. Further, the entanglement is found to be robust against small perturbations in the tuning parameters, which need only be approximately symmetric (couplings, drivings) or antisymmetric (detunings) to generate high concurrence states.

We also examine entanglement detection by an antibunching signature in the second-order correlation function that is routinely measured by means of a Hanbury-Brown-Twiss interferometer. By correlating this effect with the steady-state concurrence, we analyze how the correlation function at zero-delay may serve as a robust entanglement signature for dissipating coupled qubit systems. Importantly, we also demonstrate that dynamics driven by weak fields allows the antibunching signature to persist on $\mathcal{O}$(ps) time scales that pave the way to experimental detection using currently available experimental techniques. This robustness against microscopic perturbations and unentangled fixed point states cements the $g^{(2)}(\tau)$ correlation function as a simple and practical measure of steady-state entanglement generation.

ACKNOWLEDGMENTS

The authors thank F. Mohiyaddin for discussions and careful reading of the manuscript. E.D. acknowledges support from the Intelligence Community Postdoctoral Research Program. Research sponsored by the Intelligence Community Postdoctoral Research Fellowship and the Laboratory Directed Research and Development Program of Oak Ridge National Laboratory, managed by UT-Battelle, LLC, for the U.S. Department of Energy. This manuscript was authored by UT-Battelle, LLC, under Contract No. DE-AC0500OR22725 with the U.S. Department of Energy.

[1] M. A. Nielsen and I. L. Chung, *Quantum Computation and Quantum Information* (Cambridge University Press, Cambridge, England, 2010).
[2] B. M. Terhal, Quantum error correction for quantum memories, Rev. Mod. Phys. **87**, 307 (2015).
[3] D. Aharonov and M. Ben-Or, *Fault-Tolerant Quantum Computation with Constant Error*, in *Proceedings of the 29th Annual ACM Symposium on Theory of Computation* (ACM, New York, 1998).
[4] P. W. Shor, Scheme for reducing decoherence in quantum computer memory, Phys. Rev. A **52**, R2493(R) (1995).
[5] A. R. Calderbank, E. M. Rains, P. W. Shor, and N. J. A. Sloane, Quantum error correction via codes over GF(4), IEEE Trans. Inform. Theory **44**, 1369 (1998).
[6] R. Laflamme, C. Miquel, J. P. Paz, and W. H. Zurek, Perfect Quantum Error Correcting Code, Phys. Rev. Lett. **77**, 198 (1996).
[7] A. M. Steane, Error Correcting Codes in Quantum Theory, Phys. Rev. Lett. **77**, 793 (1996).
[8] D. Gottesman, Stabilizer codes and quantum error correction, arXiv:quant-ph/9705052.
[9] A. Y. Kitaev, Fault-tolerant quantum computation by anyons, Ann. Phys. (NY) **303**, 2 (2003).
[10] L. Viola, E. Knill, and S. Lloyd, Dynamical Decoupling of Open Quantum Systems, Phys. Rev. Lett. **82**, 2417 (1999).
[11] A. C. Doherty, S. Habib, K. Jacobs, H. Mabuchi, and S. M. Tan, Quantum feedback control and classical control theory, Phys. Rev. A **62**, 012105 (2000).
[12] D. Dong and I. R. Petersen, Quantum control theory and applications: A survey, IET Control Theory & Appl. **4**, 2651 (2010).
[13] F. Verstraete, M. M. Wolf, and J. I. Cirac, Quantum computation and quantum-state engineering driven by dissipation, Nat. Phys. **5**, 633 (2009).
[14] F. Reiter, M. J. Kastoryano, and A. S. Sorensen, Driving two atoms in an optical cavity into an entangled steady state using engineered decay, New J. Phys. **14**, 053022 (2012).
[15] M. J. Kastoryano, M. M. Wolf, and J. Eisert, Precisely Timing Dissipative Quantum Information Processing, Phys. Rev. Lett. **110**, 110501 (2013).
[16] Y. Lin, J. P. Gaebler, F. Reiter, T. R. Tan, R. Bowler, A. S. Sorensen, D. Leibfried, and D. J. Wineland, Dissipative production of a maximally entangled steady state of two quantum bits, Nature **504**, 415 (2013).
[17] C. A. Muschik, E. S. Polzik, and J. I. Cirac, Dissipatively driven entanglement of two macroscopic atomic ensembles, Phys. Rev. A **83**, 052312 (2011).
[18] H. Krauter, C. A. Muschik, K. Jensen, W. Wasilewski, J. M. Petersen, J. Ignacio Cirac, and E. S. Polzik, Entanglement Generated by Dissipation and Steady State Entanglement of Two Macroscopic Objects, Phys. Rev. Lett. **107**, 080503 (2011).
[19] Y. Liu, S. Shankar, N. Ofek, M. Hatridge, A. Narla, K. M. Sliwa, L. Frunzio, R. J. Schoelkopf, and M. H. Devoret, Comparing and Combining Measurement-Based and Driven-Dissipative Entanglement Stabilization, Phys. Rev. X **6**, 011022 (2016).

[20] M. S. Tame, K. R. McEnery, S. K. Ozdemir, J. Lee, S. A. Maier, and M. S. Kim, Quantum plasmonics, Nat. Phys. **9**, 329 (2013).
[21] P. Ginzburg, Cavity quantum electrodynamics in application to plasmonics and metamaterials, Reviews in Physics **1**, 120 (2016).
[22] E. Altewischer, M. P. van Exter, and J. P. Woerdman, Plasmon-assisted transmission of entangled photons, Nature **418**, 304 (2002).
[23] B. J. Lawrie, P. G. Evans, and R. C. Pooser, Extraordinary Optical Transmission of Multimode Quantum Correlations via Localized Surface Plasmons, Phys. Rev. Lett. **110**, 156802 (2013).
[24] M. W. Holtfrerich, M. Dowran, R. Davidson, B. J. Lawrie, R. C. Pooser, and A. M. Marino, Toward quantum plasmonic networks, Optica **3**, 985 (2016).
[25] W. Fan, B. J. Lawrie, and R. C. Pooser, Quantum plasmonic sensing, Phys. Rev. A **92**, 053812 (2015).
[26] R. C. Pooser and B. Lawrie, Plasmonic trace sensing below the photon shot noise limit, ACS Photonics **3**, 8 (2016).
[27] G. M. Akselrod *et al.*, Probing the mechanisms of large Purcell enhancement in plasmonic nanoantennas, Nat. Photonics **8**, 835 (2014).
[28] K. Santhosh, O. Bitton, L. Chuntonov, and G. Haran, Vacuum Rabi splitting in a plasmonic cavity at the single quantum emitter limit, Nat. Commun. **7**, 11823 (2016).
[29] R. Chikkaraddy *et al.*, Single-molecule strong coupling at room temperature in plasmonic nanocavities, Nature **535**, 127 (2016).
[30] T. Hummer, F. J. Garcia-Vidal, L. Martin-Moreno, and D. Zueco, Weak and strong coupling regimes in plasmonic QED, Phys. Rev. B **87**, 115419 (2013).
[31] G.-Y. Chen, N. Lambert, C.-H. Chou, Y.-N. Chen, and F. Nori, Surface plasmons in a metal nanowire coupled to colloidal quantum dots: Scattering properties and quantum entanglement, Phys. Rev. B **84**, 045310 (2011).
[32] J. Ren, T. Wu, and X. Zhang, Multifrequency multi-qubit entanglement based on plasmonic hot spots, Sci. Rep. **5**, 13941 (2015).
[33] J. Hakami and M. S. Zubairy, Nanoshell-mediated robust entanglement between coupled quantum dots, Phys. Rev. A **93**, 022320 (2016).
[34] A. Gonzalez-Tudela, F. J. Rodríguez, L. Quiroga, and C. Tejedor, Dissipative dynamics of a solid-state qubit coupled to surface plasmons: From non-Markov to Markov regimes, Phys. Rev. B **82**, 115334 (2010).
[35] C. Lee, M. Tame, C. Noh, J. Lim, S. A. Maier, J. Lee, and D. G. Angelakis, Robust-to-loss entanglement generation using a quantum plasmonic nanoparticle array, New Jour. Phys. **15**, 083017 (2013).
[36] S. A. H. Gangaraj, A. Nemilentsau, G. W. Hanson, and S. Hughes, Transient and steady-state entanglement mediated by three-dimensional plasmonic waveguides, Opt. Express **23**, 22330 (2015).
[37] K. V. Nerkararyan and S. I. Bozhevolnyi, Entanglement of two qubits mediated by a localized surface plasmon, Phys. Rev. B **92**, 045410 (2015).
[38] M. Otten, R. A. Shah, N. F. Scherer, M. Min, M. Pelton, and S. K. Gray, Entanglement of two, three, or four plasmonically coupled quantum dots, Phys. Rev. B **92**, 125432 (2015).
[39] M. Otten, J. Larson, M. Min, S. M. Wild, M. Pelton, and S. K. Gray, Origins and optimization of entanglement in plasmonically coupled quantum dots, Phys. Rev. A **94**, 022312 (2016).
[40] D. Martin-Cano, A. Gonzalez-Tudela, L. Martin-Moreno, F. J. Garcia-Vidal, C. Tejedor, and E. Moreno, Dissipation-driven generation of two-qubit entanglement mediated by plasmonic waveguides, Phys. Rev. B **84**, 235306 (2011).
[41] A. Gonzalez-Tudela, D. Martin-Cano, E. Moreno, L. Martin-Moreno, C. Tejedor, and F. J. Garcia-Vidal, Entanglement of Two Qubits Mediated by One-Dimensional Plasmonic Waveguides, Phys. Rev. Lett. **106**, 020501 (2011).
[42] J. Hou, K. Slowik, F. Lederer, and C. Rockstuhl, Dissipation-driven entanglement between qubits mediated by plasmonic nanoantennas, Phys. Rev. B **89**, 235413 (2014).
[43] R. Hanson, L. P. Kouwenhoven, J. R. Petta, S. Tarucha, and L. M. K. Vandersypen, Spins in few-electron quantum dots, Rev. Mod. Phys. **79**, 1217 (2007).
[44] P. Lodahl, S. Mahmoodian, and S. Stobbe, Interfacing single photons and single quantum dots with photonic nanostructures, Rev. Mod. Phys. **87**, 347 (2015).
[45] D. E. Chang, A. S. Sørensen, P. R. Hemmer, and M. D. Lukin, Quantum Optics with Surface Plasmons, Phys. Rev. Lett **97**, 053002 (2006).
[46] J. A. Dionne, L. A. Sweatlock, H. A. Atwater, and A. Polman, Plasmon slot waveguides: Towards chip-scale propagation with subwavelength-scale localization, Phys. Rev. B **73**, 035407 (2006).
[47] F. Benz *et al.*, Single-molecule optomechanics in "picocavities", Science **354**, 726 (2016).
[48] R. B. Davidson II, A. Yanchenko, J. I. Ziegler, S. M. Avanesyan, B. J. Lawrie, and R. F. Haglund, Jr., Ultrafast plasmonic control of second harmonic generation, ACS Photonics **3**, 1477 (2016).
[49] W. K. Wooters, Entanglement of Formation of an Arbitrary State of Two Qubits, Phys. Rev. Lett. **80**, 2245 (1998).
[50] M. W. Doherty, N. B Manson, P. Delaney, F. Jelezko, J. Wrachtrip, and C. L. Hollenberg, The nitrogen-vacancy color center in diamond, Phys. Rep. **528**, 1 (2013).
[51] J. F. Poyatos, J. I. Cirac, and P. Zoller, Complete Characterization of a Quantum Process: The Two-Bit Quantum Gate, Phys. Rev. Lett. **78**, 390 (1997).
[52] I. L. Chuang and M. A. Nielsen, Prescription for experimental determination of the dynamics of a quantum black box, J. Mod. Opt. **44**, 2455 (1997).
[53] J. S. Bell, On the Einstein Podolsky Rosen paradox, Physics **1**, 195 (1964).
[54] J. F. Clauser, M. A. Horne, A. Shimony, and R. A. Holt, Proposed Experiment to Test Local Hidden-Variable Theories, Phys. Rev. Lett. **23**, 880 (1969).
[55] H. Zheng and H. U. Baranger, Persistent Quantum Beats and Long-Distance Entanglement from Waveguide-Mediated Interactions, Phys. Rev. Lett. **110**, 113601 (2013).
[56] N. Thakkar, C. Cherqui, and D. J. Masiello, Quantum beats from entangled localized surface plasmons, ACS Photonics **2**, 157 (2015).
[57] R. Hanbury Brown and R. Q. Twiss, A test of a new type of stellar interferometer on sirius, Nature **178**, 1046 (1956).